

Higher order approximations to the longitudinal structure function F_L from the parametrization of F_2 based on the Laplace transformation

G.R.Boroun* and B.Rezaei†

Department of Physics, Razi University, Kermanshah 67149, Iran

(Dated: February 1, 2022)

We describe the determination of the longitudinal structure function F_L at NLO and NNLO approximations, using Laplace transform techniques, into the parametrization of $F_2(x, Q^2)$ and its derivative with respect to $\ln Q^2$ at low values of the Bjorken variable x . The obtained results are comparable with others by considering the effect of the charm quark mass to the longitudinal structure function, which leads to rescaling variable for $n_f = 4$. Numerical calculations and comparison with H1 data demonstrate that the suggested method provides reliable $F_L(x, Q^2)$ at small x in a wide range of Q^2 values and can be applied as well in analyses of ultra-high energy processes with cosmic neutrinos. The obtained longitudinal structure functions with and without the LHeC simulated uncertainties [CERN-ACC-Note-2020-0002, arXiv:2007.14491 [hep-ex] (2020)] are compared with the H1 Collaboration data [Eur.Phys.J.C74, 2814(2014) and Eur.Phys.J.C71, 1579 (2011)] and with the results from CT18 [Phys.Rev.D103, 014013(2021)] parametrization model at NLO and NNLO approximations.

Introduction

In recent years, many attempts have been made to better understand the longitudinal structure function experimentally and theoretically [1-8]. In perturbative quantum chromodynamics (pQCD), the longitudinal structure function contains information about the gluon distribution and strong interaction dynamics. Thus a measurement of the longitudinal proton structure function provide a unique test of parton dynamics and the consistency of QCD to the gluon density. The longitudinal structure function can be extracted from the inclusive cross section only in the region of large inelasticity y . At HERA, the measurement of the longitudinal structure function collected about 5.9 and 12.2 Pb^{-1} of data at reduced beam energies which data were analysed together with about 100 Pb^{-1} at nominal HERA energies [9]. In ultra-high energy processes, at extremely small x , the longitudinal structure function becomes predominant and its behavior will be checked in high energy process such as the Large Hadron electron Collider (LHeC) and the Future Circular Collider electron-hadron (FCC-eh) projects which runs to beyond a TeV in center-of-mass energy [9]. In the future the electron-proton colliders will be generated and extended much lower values of x and high values of Q^2 . The simultaneous measurement of the longitudinal structure functions is the cleanest way to establish new gluon density at small x . An important advantage of future colliders, compared to HERA experiments, is the wide range of y values covered until 0.9. Indeed the longitudinal structure function measurement will cover an

range from 2×10^{-6} to above $x = 0.01$ which the LHeC promises to provide. As it extends the kinematic range in electron-proton (ep) scattering by nearly four orders of magnitude of ep collisions at HERA [10]. The interest in a measurement of the longitudinal structure function, especially at small x , is related to the uncertainty in the determination of the gluon distribution. In this paper we deduce the longitudinal structure function directly to the proton structure function uncertainty.

The longitudinal structure function is directly related to the singlet and gluon distributions in the proton and its behavior have been predicted by Altarelli and Martinelli [11] equation. Authors in Ref.[11] derived an elegant formula for the longitudinal structure function $F_L(x, Q^2)$, also an effect of order $\alpha_s(Q^2)$, as a convolution integral over $F_2(x, Q^2)$ and the gluon density $g(x, Q^2)$ by the following form

$$F_L(x, Q^2) = C_{L,ns+s}(a_s(Q^2), x) \otimes F_2(x, Q^2) + \langle e^2 \rangle C_{L,g}(a_s(Q^2), x) \otimes G(x, Q^2), (1)$$

where $a_s(Q^2) = \frac{\alpha_s(Q^2)}{4\pi}$ and the non-singlet densities become negligibly small in comparison with the singlet densities at small x . Here $G(x, Q^2) = xg(x, Q^2)$ represents the gluon distribution function, $\langle e^2 \rangle$ is the average of the charge e^2 for the active quark flavors, $\langle e^2 \rangle = n_f^{-1} \sum_{i=1}^{n_f} e_i^2$ and the symbol \otimes denotes convolution according to the usual prescription. $C_{L,i}$ ($i = s, ns, g$)-s are the coefficient function which can be written by the perturbative expansion as follows [12]

$$C_{L,i}^{(\varphi)}(a_s, x) = \sum_{\phi=0}^{\varphi} a_s^{\phi+1}(Q^2) c_{L,i}^{(\phi)}(x)$$

where ϕ denotes the order in running coupling $\alpha_s(Q^2)$. According to the DGLAP Q^2 -evolution equations, the

*Electronic address: grboroun@gmail.com; boroun@razi.ac.ir

†brezaei@razi.ac.ir

singlet distribution function leads to the following relation of integro-differential equation

$$\frac{\partial F_2(x, Q^2)}{\partial \ln Q^2} = -\frac{a_s(Q^2)}{2} [P_{qq}(x) \otimes F_2(x, Q^2) + \langle e^2 \rangle P_{qg}(x) \otimes xg(x, Q^2)], \quad (2)$$

where

$$P_{a,b}(x) = P_{a,b}^{(0)}(x) + a_s(Q^2) \tilde{P}_{a,b}^{(1)}(x) + a_s^2(Q^2) \tilde{P}_{a,b}^{(2)}(x) \quad (3)$$

and

$$\tilde{P}_{ab}^{(n)}(x) = P_{ab}^{(n)}(x) + [C_{2,s} + C_{2,g} + \dots] \otimes P_{ab}^{(0)}(x) + \dots$$

The quantities \tilde{P}_{ab} 's are expressed via the known splitting and Wilson coefficient functions in literatures [13,14].

Recently authors in Ref.[4] revives the parametrization of the longitudinal structure function at next-to-leading order (NLO) approximation by using the parametrization of the proton structure function $F_2(x, Q^2)$ where suggested by authors in Ref.[15] by a fit to HERA data on deep-inelastic lepton-nucleon scattering (DIS) at small x . The parametrization of $F_2(x, Q^2)$ is relevant in investigations of ultra-high energy processes. Indeed authors in Ref.[4] have obtained an analytical relation for the longitudinal structure function at NLO approximation with respect to the Mellin transform method, by the following form

$$F_L^{\text{NLO}}(x, Q^2) = \tau(a_s) \{ \vartheta(a_s) F_L^{\text{LO}}(x, Q^2) - \chi(a_s^2) F_2(x, Q^2) \}, \quad (4)$$

where

$$\begin{aligned} F_L^{\text{LO}}(x, Q^2) &= (1-x)^n \sum_{\varepsilon=0}^2 C_\varepsilon(Q^2) L^\varepsilon \\ \tau(a_s) &= [1 + \frac{1}{3} a_s(Q^2) L_C (\hat{\delta}_{sg}^{(1)} - \hat{R}_{L,g}^{(1)})]^{-1} \\ \vartheta(a_s) &= [1 - a_s(Q^2) (\bar{\delta}_{sg}^{(1)} - \bar{R}_{L,g}^{(1)})] \\ \chi(a_s^2) &= a_s^2(Q^2) [\frac{1}{3} \hat{B}_{L,s}^{(1)} L_A + \bar{B}_{L,s}^{(1)}], \end{aligned} \quad (5)$$

and

$$F_2(x, Q^2) = D(Q^2) (1-x)^n \sum_{\varepsilon=0}^2 A_\varepsilon(Q^2) L^\varepsilon. \quad (6)$$

Here L 's are the logarithmic terms. The coefficient functions at LO and NLO approximations are summarized in Appendix A and the effective parameters are defined in Table I.

In this article we investigate the behavior of the longitudinal structure function inside the proton at high-order

corrections to the running coupling by using the Laplace transform techniques at small x . Indeed, we use the Laplace-transform technique for solving the Altarelli-Martinelli equation by employing the parametrization of $F_2(x, Q^2)$ at next-to-leading order (NLO) and next-to-next-to-leading order (NNLO) approximations. We demonstrate that the small x behavior of longitudinal structure function can be directly related to the known structure function $F_2(x, Q^2)$ (i.e., Eq.(6)) and known its derivative $\partial F_2(x, Q^2)/\partial \ln Q^2$ at the higher order approximations.

Method

Considering the variable definitions $v \equiv \ln(1/x)$ and $w \equiv \ln(1/z)$, one can rewrite the equations (1) and (2) in terms of the convolution integrals and new variables, as

$$\frac{\partial \hat{\mathcal{F}}_2(v, Q^2)}{\partial \ln Q^2} = \int_0^v [\hat{\mathcal{F}}_2(v, Q^2) \hat{\mathcal{H}}_{2,s}^{(\varphi)}(a_s(Q^2), v-w) + \langle e^2 \rangle \hat{\mathcal{G}}(v, Q^2) \hat{\mathcal{H}}_{2,g}^{(\varphi)}(a_s(Q^2), v-w)] dw, \quad (7)$$

$$\hat{\mathcal{F}}_L(v, Q^2) = \int_0^v [\hat{\mathcal{F}}_2(v, Q^2) \hat{\mathcal{K}}_{L,s+n_s}^{(\varphi)}(a_s(Q^2), v-w) + \langle e^2 \rangle \hat{\mathcal{G}}(v, Q^2) \hat{\mathcal{K}}_{L,g}^{(\varphi)}(a_s(Q^2), v-w)] dw, \quad (8)$$

where

$$\begin{aligned} \hat{\mathcal{F}}_L(v, Q^2) &\equiv F_L(e^{-v}, Q^2), \\ \frac{\partial \hat{\mathcal{F}}_2(v, Q^2)}{\partial \ln Q^2} &\equiv \frac{\partial F_2(e^{-v}, Q^2)}{\partial \ln Q^2}, \\ \hat{\mathcal{G}}(v, Q^2) &\equiv G(e^{-v}, Q^2), \\ \hat{\mathcal{H}}^{(\varphi)}(a_s(Q^2), v) &\equiv e^{-v} \hat{P}_{a,b}^{(\varphi)}(a_s(Q^2), v), \\ \hat{\mathcal{K}}^{(\varphi)}(a_s(Q^2), v) &\equiv e^{-v} \hat{C}_{L,i}^{(\varphi)}(a_s(Q^2), v). \end{aligned}$$

The Laplace transform of $\hat{\mathcal{H}}(a_s(Q^2), v)$'s and $\hat{\mathcal{K}}(a_s(Q^2), v)$'s are given by the following forms

$$\begin{aligned} \Phi_f^{(\varphi)}(a_s(Q^2), s) &\equiv \mathcal{L}[\hat{\mathcal{H}}_{2,s}^{(\varphi)}(a_s(Q^2), v); s] \\ &= \int_0^\infty \hat{\mathcal{H}}_{2,s}^{(\varphi)}(a_s(Q^2), v) e^{-sv} dv, \\ \Theta_f^{(\varphi)}(a_s(Q^2), s) &\equiv \mathcal{L}[\hat{\mathcal{H}}_{2,g}^{(\varphi)}(a_s(Q^2), v); s] \\ &= \int_0^\infty \hat{\mathcal{H}}_{2,g}^{(\varphi)}(a_s(Q^2), v) e^{-sv} dv, \\ \Phi_L^{(\varphi)}(a_s(Q^2), s) &\equiv \mathcal{L}[\hat{\mathcal{K}}_{L,s+n_s}^{(\varphi)}(a_s(Q^2), v); s] \\ &= \int_0^\infty \hat{\mathcal{K}}_{L,s+n_s}^{(\varphi)}(a_s(Q^2), v) e^{-sv} dv, \\ \Theta_L^{(\varphi)}(a_s(Q^2), s) &\equiv \mathcal{L}[\hat{\mathcal{K}}_{L,g}^{(\varphi)}(a_s(Q^2), v); s] \\ &= \int_0^\infty \hat{\mathcal{K}}_{L,g}^{(\varphi)}(a_s(Q^2), v) e^{-sv} dv, \end{aligned}$$

with the condition $\widehat{\mathcal{H}}(v) = 0$ and $\widehat{\mathcal{K}}(v) = 0$ for $v = 0$ [16]. The convolution theorem for Laplace transforms allows us to rewrite the right hand sides of Eqs.(7) and (8) with considering the fact that the Laplace transform of the convolution factors are simply the ordinary product of the Laplace transform of the factors. Consequently, we can obtain the equations for the structure functions in the Laplace space s by the following forms as

$$\begin{aligned} \frac{\partial f_2(s, Q^2)}{\partial \ln Q^2} &= \Phi_f^{(\varphi)}(a_s(Q^2), s) f_2(s, Q^2) \\ &\quad + \langle e^2 \rangle \Theta_f^{(\varphi)}(a_s(Q^2), s) g(s, Q^2), \\ f_L(s, Q^2) &= \Phi_L^{(\varphi)}(a_s(Q^2), s) f_2(s, Q^2) \\ &\quad + \langle e^2 \rangle \Theta_L^{(\varphi)}(a_s(Q^2), s) g(s, Q^2), \end{aligned} \quad (9)$$

where

$$\begin{aligned} \mathcal{L}[\widehat{\mathcal{F}}_L(v, Q^2); s] &= f_L(s, Q^2), \\ \mathcal{L}[\widehat{\mathcal{F}}_2(v, Q^2); s] &= f_2(s, Q^2), \end{aligned}$$

and

$$\begin{aligned} \eta_j^{(\varphi)}(a_s(Q^2), s) &= \sum_{\phi=0}^{\varphi} a_s^{\phi+1}(Q^2) \eta_j^{(\phi)}(s), \\ \eta &= (\Phi, \Theta), \quad j = (f, L), \end{aligned}$$

where the superscript of the kernels represents the order in α_s . The leading-order coefficient functions Φ and Θ in the Laplace space s are given by

$$\begin{aligned} \Phi_L^{(0)}(s) &= 4C_F \frac{1}{2+s}, \\ \Theta_L^{(0)}(s) &= 8n_f \left(\frac{1}{2+s} - \frac{1}{3+s} \right), \\ \Theta_f^{(0)}(s) &= 2n_f \left(\frac{1}{1+s} - \frac{2}{2+s} + \frac{2}{3+s} \right), \\ \Phi_f^{(0)}(s) &= 4 - \frac{8}{3} \left(\frac{1}{1+s} + \frac{1}{2+s} \right) + 2(\psi(s+1) + \gamma_E), \end{aligned} \quad (10)$$

where $\psi(x)$ is the digamma function and $\gamma_E = 0.5772156\dots$ is Euler constant.

Defining $\psi(s+1) + \gamma_E = S_1(s)$ and using the notion of the so-called nested sums [4,17]. Let us to study the well known function

$$S_a(s) = \sum_{m=1}^s \frac{1}{m^a},$$

where for the case $a \geq 2$ is defined by the following form

$$\begin{aligned} S_a(s) &= \left[\sum_{m=1}^{\infty} - \sum_{m=s}^{\infty} \right] \frac{1}{m^a} = S_a(\infty) - \sum_{l=s+1}^{\infty} \frac{1}{(l+s+1)^a} \\ &\equiv S_a(\infty) - \Psi_a(s+1). \end{aligned} \quad (11)$$

Here $S_a(\infty) = \zeta(a)$ where $\zeta(a)$ is the Riemann zeta function and $\Psi_a(s+1) = \frac{(-1)^a}{(a-1)!} \Psi^{(a-1)}(s+1)$ where $\Psi^{(a)}(s)$

is a -time derivative of the Euler Ψ -function. Now let us to continue with the function

$$S_{-a}(s) = \sum_{m=1}^s \frac{(-1)^m}{m^a},$$

where by analogy with Eq.(11) we have that

$$\begin{aligned} S_{-a}(s) &= \left[\sum_{m=1}^{\infty} - \sum_{m=s}^{\infty} \right] \frac{(-1)^m}{m^a} \\ &= S_{-a}(\infty) - \sum_{l=s+1}^{\infty} \frac{(-1)^{l+s+1}}{(l+s+1)^a} \\ &\equiv S_{-a}(\infty) - (-1)^s \Psi_{-a}(s+1), \end{aligned} \quad (12)$$

with $S_{-1}(\infty) = -\ln 2$ and $S_{-a}(\infty) = \zeta(-a) = (2^{1-a} - 1)\zeta(a)$ [17]. By analogy with Eqs.(11) and (12), authors in Ref.[4] show that the functions $S_1(s)$ and $S_{-1}(s)$ ones lead to the following functions respectively

$$\begin{aligned} S_1(s) &= \Psi(s+1) - \Psi(1), \\ S_{-1}(s) &= -\ln(2) - \sum_{l=0}^{\infty} \frac{(-1)^{l+1}}{s+l+1}. \end{aligned} \quad (13)$$

The above equation indicates that for large l 's, the function is convergent, which is well known for any values of s . In the following we use the procedure of analytic continuation for the sums $S_1(s)$, which come in consideration of the parton distribution functions.

All further theoretical details relevant for analyzing F_L at NLO and NNLO in the $\overline{\text{MS}}$ factorization scheme have been presented in Refs.[18-21]. The explicit expressions for the NLO and NNLO kernels in s -space are rather cumbersome, therefore we recall that we are interested in investigation of the kernels in small x [12, 18-21]. In the Laplace space we consider the kernels at small s , as the two and three-loop kernels read

$$\begin{aligned} \Phi_{L,s \rightarrow 0}^{(1)}(s) &\simeq n_f \left[-\frac{2.371}{s} \right], \\ \Theta_{L,s \rightarrow 0}^{(1)}(s) &\simeq n_f \left[-\frac{5.333}{s} \right], \\ \Theta_{f,s \rightarrow 0}^{(1)}(s) &\simeq C_A T_f \left[\frac{40}{9s} \right], \\ \Phi_{f,s \rightarrow 0}^{(1)}(s) &\simeq C_F T_f \left[\frac{40}{9s} \right], \end{aligned} \quad (14)$$

and

$$\begin{aligned} \Phi_{L,s \rightarrow 0}^{(2)}(s) &\simeq n_f \left[-\frac{885.530}{s} + \frac{182}{s^2} \right] + n_f^2 \left[\frac{40.239}{s} \right], \\ \Theta_{L,s \rightarrow 0}^{(2)}(s) &\simeq n_f \left[-\frac{2044.700}{s} + \frac{409.506}{s^2} \right] + n_f^2 \left[\frac{88.504}{s} \right], \\ \Theta_{f,s \rightarrow 0}^{(2)}(s) &\simeq n_f \left[-\frac{1268.300}{s} + \frac{896}{3s^2} \right] + n_f^2 \left[\frac{1112}{243s} \right], \\ \Phi_{f,s \rightarrow 0}^{(2)}(s) &\simeq n_f \left[-\frac{506}{s} + \frac{3584}{27s^2} \right] + n_f^2 \left[\frac{256}{81s} \right]. \end{aligned} \quad (15)$$

The standard representation for QCD couplings in NLO and NNLO (within the $\overline{\text{MS}}$ -scheme) approximations have the forms

$$\begin{aligned}\alpha_s(t) &= \frac{4\pi}{\beta_0 t} \left[1 - \frac{\beta_1}{\beta_0^2} \frac{\ln t}{t} \right] & (\text{NLO}), \\ \alpha_s(t) &= \frac{4\pi}{\beta_0 t} \left[1 - \frac{\beta_1}{\beta_0^2} \frac{\ln t}{t} \right. \\ &\quad \left. + \frac{1}{\beta_0^3 t^2} \left\{ \frac{\beta_1^2}{\beta_0} (\ln^2 t - \ln t - 1) + \beta_2 \right\} \right] & (\text{NNLO}),\end{aligned}$$

where β_0 , β_1 and β_2 are the one, two and three loop correction to the QCD β -function and $t = \ln \frac{Q^2}{\Lambda^2}$, Λ is the QCD cut-off parameter.

Consequently, by working in the Laplace space s , we can obtain the longitudinal structure function by solving Eq.(9) for $f_L(s, Q^2)$ into $f_2(s, Q^2)$ and $\partial f_2(s, Q^2)/\partial \ln Q^2$ as

$$\begin{aligned}f_L(s, Q^2) &= k^{(\varphi)}(a_s(Q^2), s) f_2(s, Q^2) \\ &\quad + h^{(\varphi)}(a_s(Q^2), s) \frac{\partial f_2(s, Q^2)}{\partial \ln Q^2},\end{aligned}\quad (16)$$

where the kernels $k^{(\varphi)}(a_s(Q^2), s)$ and $h^{(\varphi)}(a_s(Q^2), s)$ contain contributions of the s -space splitting and coefficient functions up to the NNLO approximation. These kernels can be evaluated from s -space results by the following forms

$$\begin{aligned}k^{(\varphi)}(a_s(Q^2), s) &= \sum_{\phi=0}^{\varphi} a_s^{\phi+1}(Q^2) \Phi_L^{(\phi)}(s) \\ &\quad - h^{(\varphi)}(a_s(Q^2), s) \sum_{\phi=0}^{\varphi} a_s^{\phi+1}(Q^2) \Phi_f^{(\phi)}(s), \\ h^{(\varphi)}(a_s(Q^2), s) &= \frac{\sum_{\phi=0}^{\varphi} a_s^{\phi+1}(Q^2) \Theta_L^{(\phi)}(s)}{\sum_{\phi=0}^{\varphi} a_s^{\phi+1}(Q^2) \Theta_f^{(\phi)}(s)}.\end{aligned}\quad (17)$$

The inverse Laplace transform of coefficients $k(a_s(Q^2), s)$ and $h(a_s(Q^2), s)$ in above equations are defined as kernels

$$\widehat{\eta}(a_s(Q^2), v) \equiv \mathcal{L}^{-1}[k(a_s(Q^2), s); v]$$

and

$$\widehat{J}(a_s(Q^2), v) \equiv \mathcal{L}^{-1}[h(a_s(Q^2), s); v]$$

respectively. Clearly the kernels (i.e., $\widehat{\eta}$ and \widehat{J}) are dependent on v and the running coupling at the higher order approximations. We will generally not be able to define an analytical form for these kernels at higher order approximations, so F_L determined by numerical integral of the parametrization of F_2 and its derivative, as

$$\begin{aligned}\widehat{F}_L(v, Q^2) &\equiv \mathcal{L}^{-1}[f_L(s, Q^2); v] & (18) \\ &= \int_0^v [\widehat{F}_2(w, Q^2) \widehat{\eta}^{(\varphi)}(a_s(Q^2), v-w) \\ &\quad + \frac{\partial \widehat{F}_2(w, Q^2)}{\partial \ln Q^2} \widehat{J}^{(\varphi)}(a_s(Q^2), v-w)] dw.\end{aligned}$$

Consequently, one can obtain the longitudinal structure function as $F_L(x, Q^2)$. Therefore the general analytical expression for the longitudinal structure function in x -space is given by

$$\begin{aligned}F_L(x, Q^2) &= \int_x^1 \frac{dy}{y} [F_2(y, Q^2) \eta^{(\varphi)}\left(\frac{x}{y}, Q^2\right) \\ &\quad + \frac{\partial F_2(y, Q^2)}{\partial \ln Q^2} J^{(\varphi)}\left(\frac{x}{y}, Q^2\right)].\end{aligned}\quad (19)$$

So that we have an explicit solution for the longitudinal structure function at NLO and NNLO approximations which can be evaluated to the numerical accuracy to which $F_2(x, Q^2)$ is known. Having an analytical proton structure function and its derivative with respect to $\ln Q^2$, one can extract the longitudinal structure function numerically at any desired x and Q^2 values.

Results and Discussion

In order to make the effect of production threshold for charm quark at $n_f = 4$ one should take into account quark mass for small Q^2 . To this end we shall follow the rescaling variable χ which introduced by Aivazis, Collins, Olness and Tung (ACOT) in Ref.[22]. Therefore, the longitudinal structure function is defined by the rescaling variable χ where

$$\chi = x \left(1 + \frac{4m_c^2}{Q^2} \right).$$

This rescaled variable is one of the ingredients used in the general-mass variable flavor number scheme (GM-VFNS), which is used in the global fits of PDFs of the CETQ and MRST groups. The running charm mass is obtained as $m_c = 1.29_{-0.053}^{+0.077}$ GeV, where the uncertainties are obtained through adding the experimental fit, model and parametrization uncertainties in quadrature [1,2]. At high Q^2 values ($m_c^2/Q^2 \ll 1$), the rescaling variable χ reduces to the Bjorken variable x as $\chi \rightarrow x$ [22,23]. The QCD parameter Λ has been extracted due to $\alpha_s(M_z^2) = 0.1166$, which for four number of active flavor is defined by $\Lambda_{\text{QCD}}^{\text{LO}} = 136.8$ MeV and $\Lambda_{\text{QCD}}^{\text{NLO}} = 284.0$ MeV. Also we take $\Lambda_{\text{QCD}}^{\text{NNLO}} = 235.0$ MeV.

Now we can proceed to extract the longitudinal structure function $F_L(x, Q^2)$ with the explicit form of the proton structure function and its derivative at NLO and NNLO approximations. In order to present more detailed discussions on our findings, the results for the longitudinal structure function compared with CT18 [24] parametrization model. It should also be mentioned that CT18 results at NLO and NNLO approximations obtained using a wide variety of high-precision Large Hadron Collider (LHC) data, in addition to the combined HERA I+II deep inelastic scattering data set. In

Fig.1 we are presented the x -dependence of the longitudinal structure function at $Q^2 = 5, 15, 25$ and 45 GeV^2 and compared with H1 Collaboration data [1,2] and the results from CT18 NLO parametrization model. The error bands illustrated in this figure, and in the other figures, are into the charm-quark mass uncertainty and the statistical errors in the parametrization of $F_2(x, Q^2)$ and its derivative, where the fit parameter errors are shown in Table I. As can be seen from the related figures, the longitudinal structure function results are consistent with the CT18 NLO and H1 Collaboration data at moderate and large values of Q^2 . It is seen that, for all values of the presented Q^2 with respect to the rescaling variable, the extracted longitudinal structure functions at NLO approximation due to the Laplace transform method are in a good agreement with data and parametrization models.

In Fig.2, the results for the longitudinal structure function within the NNLO approximation have been shown and compared with the NNLO analysis of CT18 model. We observe that, with respect to the approximation approach used in the coefficient functions at higher order approximation in the limit $x \rightarrow 0$, the extracted longitudinal structure functions within the NNLO approximation are comparable with the experimental data and the CT18 NNLO model. These results are interesting in connection with theoretical investigations of ultra-high energy processes with cosmic neutrinos.

In Fig.3 the longitudinal structure function results at NLO and NNLO approximations due to the Laplace transforms method are associated with the LHeC simulated uncertainties. These simulated uncertainties for the longitudinal structure function measurement recently reported by the LHeC Collaboration and FCC-he Study Group in Ref.[9]. In this figure the straight lines represent the CT18 NLO and CT18 NNLO QCD analysis in different schemes and the up and down triangles represent our results as accompanied with the LHeC simulated uncertainties. We compare the results for the longitudinal structure function at NLO and NNLO approximations with a general-mass variable-flavor-number scheme (GM-VFNS) and zero-mass variable-flavor-number scheme (ZM-VFNS) in the CT18 NLO and NNLO methods in this figure respectively. As can be seen from the related figures, the longitudinal structure function results are consistent with different schemes in the CT18 NLO and NNLO at moderate and large values of Q^2 .

In Fig.4, we show the Q^2 -dependence of the longitudinal structure function at small x at NLO approximation. In this figure (i.e., Fig.4) the results of calculations and comparison with the H1 collaboration data [1,2] are presented. These results have been performed at fixed value of the invariant mass W as $W = 230 \text{ GeV}$. Over a wide range of the variable Q^2 , the extracted longitudinal structure functions at NLO approximation are in a good agreement with experimental data and CT18 NLO

analysis. For $Q^2 < 1 \text{ GeV}^2$, the extracted results have the same CT18 NLO behavior, but there are no data to compare in this region. The error bands illustrated in this figure are into the charm-quark mass uncertainty and the statistical errors in the parametrization of $F_2(x, Q^2)$, where the fit parameter errors are shown in Table I.

The longitudinal structure function behavior with the NNLO approximation is shown in Fig.5 for a wide range of Q^2 . These results in Fig.5 compared with the H1 collaboration data [1,2] and CT18 NNLO. As can be seen in this figure, these results based on the Laplace transforms method are comparable with the CT18 NNLO analysis. However, at extremely low momenta, $Q^2 < 1 \text{ GeV}^2$, the extracted F_L within NNLO approximation is below the experimental data. In this region the depletion and enhancement of F_L have the same behavior in comparison with the CT18 NNLO model. One wishes to improve substantially the precision of the F_L data with extension of kinematic range at the LHeC and FCC-eh for testing theory at small x and small Q^2 values. As commented in Refs.[9,25], resummation of the large $\ln(1/x)$ terms restore the dominance of the gg splitting over the qg one. The resummation of $(\alpha_s \ln s)^n$ series in the leading logarithmic order is a differential equation in $\ln(1/x)$ for small x evolution equation. The leading logarithmic (LLx) results yielded a growth of the gluon density and the next-to-leading logarithmic (NLLx) calculation yielded some instability in the cross sections. The appearance of the large negative corrections at NLLx motivated the longitudinal structure functions for the appropriate resummation which would stabilize the results. It was demonstrated that the resummed fits provide a better description of the longitudinal structure function data than the pure method based fits at fixed NNLO approximation. Such effects will be strongly magnified at the LHeC, as it was shown that the description of the longitudinal structure function from HERA data is improved in the fits with the small x resummation. This analysis suggests that the small x resummation effects will be visible in the small x and small Q^2 region. Indeed the longitudinal structure function in this region at NNLO approximation increase due to the resummation predictions as x decreases.

In Fig.6 the longitudinal structure function results at NLO and NNLO approximations are compared with the Regge-like behavior of the parton distribution functions. In Ref.[26] authors extracted a formula for the longitudinal structure function F_L as function of F_2 and its derivative at small x at LO and NLO approximations based on the Regge-like behavior. The Regge-like behavior for the singlet and gluon distribution functions at small x is given by

$$G(x, Q^2) = x^{-\delta} \tilde{G}(x, Q^2), \quad F_2(x, Q^2) = x^{-\delta} \tilde{s}(x, Q^2)$$

where the δ value obtained by fixed coupling LLx BFKL gives $\delta \simeq 0.5$, which is the so-called hard-Pomeron expo-

ment. This value was obtained in the studies performed in Ref. [27] as the sum of the leading powers of $\ln(1/x)$ in all orders of perturbation theory. In tensor-Pomeron model [28], where in addition to the soft tensor Pomeron a hard tensor Pomeron and Reggeon exchange included, the hard-Pomeron intercept was determined to be $\delta \simeq 0.3$. In Fig.6 our results compared with the longitudinal structure function extracted in Ref.[26] based on the parameterization of F_2 (i.e., Eq.6). We compared these results with the H1 collaboration data [1,2] and the Regge-like behavior in Ref.[26] at $Q^2 = 20 \text{ GeV}^2$. The results at NLO and NNLO approximations are comparable with the H1 collaboration data.

Finally we analysis the coefficient functions at NLO and NNLO approximations for the behavior of the longitudinal structure functions at small x in Fig.7. Authors in Refs.[18,29] considered the dynamical and standard distributions at small x . The gluon distribution at dynamical has a steeper behavior at small x in comparison with the standard model. Also the sea distribution has a similar behavior at the standard and dynamical models. Authors shown that at NLO approximation the longitudinal structure function in dynamically distribution is larger than the NNLO one for $Q^2 \geq 5 \text{ GeV}^2$ at small x . A similar behavior prevails for the longitudinal structure function in Fig.3 at moderate and large Q^2 due to the results of CT18 NLO and NNLO approximations in the GM-VFNS and ZM-VFNS. The coefficient functions in (14) and (15) are shown in Fig.7 at s -space. The behavior of the coefficient functions is considered at NLO and NNLO approximations for $s \geq 0$. It is evidence from these behaviors in Fig.7 that at NNLO the longitudinal structure function values are less than the F_L -values at NLO. Also the leading twist-2 predictions are necessary for illustrate of the longitudinal structure function behavior at $Q^2 < 5 \text{ GeV}^2$.

In conclusion, we have presented a certain theoretical model at NLO and NNLO approximations to describe the longitudinal structure function based on the Laplace transforms method at small values of x . Indeed, there are various methods to solve the Altarelli-Martinelli equation to obtain the longitudinal structure function, in this manuscript we have shown that the method of the Laplace transforms technique is also the reliable and alternative scheme to solve Altarelli-Martinelli equation, analytically. A detailed analysis has been performed to find an analytical solution of the longitudinal structure function into the parametrization of $F_2(x, Q^2)$ and its derivative of the proton structure function with respect to $\ln Q^2$ at high-order corrections. The calculations are consistent with the H1 data from HERA collider and they are comparable with the CT18 at NLO and NNLO approximations. Also we compared the longitudinal structure functions with respect to the LHeC simulated uncertainties with the CT18 at NLO and NNLO approximations due to the GM-VFN and ZM-VFN schemes.

This persuades us that the obtained results can be extended to high energy regime in new colliders (like in the proposed LHeC and FCC-eh colliders). These results indicate that the obtained solutions from present analysis at NLO and NNLO approximations based on Laplace transform technique are comparable with the ones obtained by global QCD analysis of CT18 from the parton distribution functions. In all figures clearly demonstrate that the extraction procedure provides correct behaviors of the extracted longitudinal structure function in both NLO and NNLO approximations. At intermediate and high Q^2 the extracted longitudinal structure functions at NLO and NNLO approximations are in a good agreement with experimental data. Indeed, for very small Q^2 values, the NNLO+NNLx resummation will be improve the longitudinal structure function behavior at NNLO approximation in the future colliders. We also showed that the obtained results from the longitudinal structure function analysis are in good agreement with those from the literature.

ACKNOWLEDGMENTS

The authors are thankful to the Razi University for financial support of this project. Also G.R.Boroun thanks M.Klein and N.Armeo for allowing access to data related to simulated errors of the longitudinal structure function at the Large Hadron electron Collider (LHeC).

Appendix A

The coefficient functions read as

$$\begin{aligned}
 C_2 &= \hat{A}_2 + \frac{8}{3}a_s(Q^2)DA_2 \\
 C_1 &= \hat{A}_1 + \frac{1}{2}\hat{A}_2 + \frac{8}{3}a_s(Q^2)D[A_1 + (4\zeta_2 - \frac{7}{2})A_2] \\
 C_0 &= \hat{A}_0 + \frac{1}{4}\hat{A}_2 - \frac{7}{8}\hat{A}_2 + \frac{8}{3}a_s(Q^2)D[A_0 + (2\zeta_2 - \frac{7}{4})A_1 \\
 &\quad + (\zeta_2 - 4\zeta_3 - \frac{17}{8})A_2], \tag{20}
 \end{aligned}$$

$$\begin{aligned}
\widehat{A}_2 &= \widetilde{A}_2 \\
\widehat{A}_1 &= \widetilde{A}_1 + 2DA_2 \frac{\mu^2}{\mu^2 + Q^2} \\
\widehat{A}_0 &= \widetilde{A}_0 + DA_1 \frac{\mu^2}{\mu^2 + Q^2} \\
\widetilde{A}_i &= \widetilde{D}A_i + D\overline{A}_i \frac{Q^2}{Q^2 + \mu^2} \\
\widetilde{D} &= \frac{M^2 Q^2 [(2 - \lambda)Q^2 + \lambda M^2]}{[Q^2 + M^2]^3} \\
\overline{A}_\varepsilon &= a_{\varepsilon 1} + 2a_{\varepsilon 2}L_2, \quad a_{02} = 0.
\end{aligned} \tag{21}$$

and

$$\begin{aligned}
\widehat{B}_{L,s}^{(1)} &= 8C_F \left[\frac{25}{9}n_f - \frac{449}{72}C_F + (2C_F - C_A) \right. \\
&\quad \left. (\zeta_3 + 2\zeta_2 - \frac{59}{72}) \right] \\
\overline{B}_{L,s}^{(1)} &= \frac{20}{3}C_F(3C_A - 2n_f) \\
\widehat{\delta}_{sg}^{(1)} &= \frac{26}{3}C_A \\
\overline{\delta}_{sg}^{(1)} &= 3C_F - \frac{347}{18}C_A \\
\widehat{R}_{L,g}^{(1)} &= -\frac{4}{3}C_A \\
\overline{R}_{L,g}^{(1)} &= -5C_F - \frac{4}{9}C_A \\
L_A &= L + \frac{A_1}{2A_2} \\
L_C &= L + \frac{C_1}{2C_2} \\
L &= \ln(1/x) + L_1 \\
L_1 &= \ln \frac{Q^2}{Q^2 + \mu^2} \\
L_2 &= \ln \frac{Q^2 + \mu^2}{\mu^2} \\
A_i(Q^2) &= \sum_{k=0}^2 a_{ik} L_2^k, \quad (i = 1, 2) \\
A_0 &= a_{00} + a_{01}L_2 \\
D &= \frac{Q^2(Q^2 + \lambda M^2)}{(Q^2 + M^2)^2},
\end{aligned} \tag{22}$$

with the color factors $C_A = 3$ and $C_F = \frac{4}{3}$ associated with the color group $SU(3)$ and n_f being the number of flavors.

TABLE I: The effective parameters at small x for $0.15 \text{ GeV}^2 < Q^2 < 3000 \text{ GeV}^2$ provided by the following values. The fixed parameters are defined by the Block-Halzen fit to the real photon-proton cross section as $M^2 = 0.753 \pm 0.068 \text{ GeV}^2$, $\mu^2 = 2.82 \pm 0.290 \text{ GeV}^2$, $n = 11.49 \pm 0.99$ and $\lambda = 2.430 \pm 0.153$ [15].

parameters	value
a_{10}	$8.205 \times 10^{-4} \pm 4.62 \times 10^{-4}$
a_{11}	$-5.148 \times 10^{-2} \pm 8.19 \times 10^{-3}$
a_{12}	$-4.725 \times 10^{-3} \pm 1.01 \times 10^{-3}$
a_{20}	$2.217 \times 10^{-3} \pm 1.42 \times 10^{-4}$
a_{21}	$1.244 \times 10^{-2} \pm 8.56 \times 10^{-4}$
a_{22}	$5.958 \times 10^{-4} \pm 2.32 \times 10^{-4}$
a_{00}	$2.550 \times 10^{-1} \pm 1.600 \times 10^{-2}$
a_{01}	$1.475 \times 10^{-1} \pm 3.025 \times 10^{-2}$

REFERENCES

1. H1 and ZEUS Collaborations (H. Abramowicz et al.), *Eur. Phys. J. C* **78**, 473 (2018).
2. H1 Collab. (V.Andreev et al.), *Eur.Phys.J.C* **74**, 2814(2014); H1 Collab. (F.D.Aaron et al.), *Eur.Phys.J.C* **71**, 1579 (2011).
3. L.P.Kaptari et al., *JETP Lett.* **109**, 281(2019).
4. L.P.Kaptari et al., *Phys.Rev.D* **99**, 096019 (2019).
5. V.Tvaskis et al., *Phys.Rev.C* **97**, 045204 (2018).
6. G.R.Boroun, arXiv: 2108.09465 [hep-ph]; *JETP Lett.* **114**, 1 (2021); *Eur.Phys.J.Plus* **135**, 68 (2020); *Phys.Rev.C* **97**, 015206 (2018).
7. M.Niedziela and M.Praszalowicz, *Acta Phys.Polon.B* **46**, 2019 (2015); N.Baruah, M.K.Das and J.K.Sarma, *Eur.Phys.J.Plus* **129**, 229 (2014); M.Mottaghizadeh and A.Mirjalili, *Phys.Lett.B* **820**, 136534 (2021); A.D.Martin, W.J.Stirling and R.S.Thorne, *Phys.Lett.B* **635**, 305 (2006); A.D.Martin, W.J.Stirling and R.S.Thorne, *Phys.Lett.B* **636**, 259 (2006); S.Zarrin and S.Dadfar, *Int.J.Theor.phys.* **60**, 3822(2021).
8. B.Rezaei and G.R.Boroun, *Eur.Phys.J.A* **56**, 262 (2020); L.Ghasemzadeh, A.Mirjalili and S.Atashbar Tehrani, *Phys.Rev.D* **104**, 074007 (2021); G.R.Boroun and B.Rezaei, *Chin.Phys.Lett.* **32**, 111101 (2015); S.S.Mohsenabadi, S.Atashbar Tehrani and F.Taghavi-Shahri, arXiv:2112.03373; G.R.Boroun, B.Rezaei and J.K.Sarma, *Int.J.Mod.Phys.A* **29**, 1450189 (2014); S.Shoeibi, F.Taghavi-Shahri, H.Khanpour and K.Javidan, *Phys.Rev.D* **97**, 074013 (2018); G.R.Boroun and B.Rezaei, *Eur.Phys.J.C* **72**, 2221 (2012); G.R.Boroun and B.Rezaei, *Phys.Letts.B* **816**, 136274 (2021); H.Khanpour, A.Mirjalili and S.Atashbar Tehrani, *Phys.Rev.C* **95**, 035201 (2017).

9. LHeC Collaboration and FCC-he Study Group, P. Agostini et al., *J. Phys. G: Nucl. Part. Phys.* **48**, 110501(2021).
- 10 M. Klein, arXiv: 1802.04317[hep-ph]; *Ann. Phys.* **528**, 138 (2016).
11. G.Altarelli and G.Martinelli, *Phys.Lett.B***76**, 89(1978).
12. S. Moch, J.A.M. Vermaseren, and A. Vogt, *Phys. Lett. B* **606**, 123 (2005).
13. J. Blumlein, V. Ravindran and W. van Neerven, *Nucl. Phys. B* **586**, 349(2000); S.Catani and F.Hautmann, *Nucl.Phys.B***427**, 475(1994).
14. D.I.Kazakov and A.V.Kotikov, *Phys.Lett.B***291**, 171(1992); E.B.Zijlstra and W.L.van Neerven, *Nucl.Phys.B*383, 525(1992).
15. M. M. Block, L. Durand and P. Ha, *Phys. Rev. D* **89**, 094027 (2014).
16. M.M.Block, *Eur.Phys.J.C* **65**, 1 (2010); M.M.Block, L.Durand and D.W.McKay, *Phys.Rev.D* **79**, 014031 (2009).
17. A. V. Kotikov and V. N. Velizhanin, arXiv: 0501274 [hep-ph] (2005); D.I.Kazakov and A.V.Kotikov, *Phys.Lett.B* **291**, 171 (1992).
18. M.Glück, C.Pisano and E.Reya, *Phys.Rev.D***77**, 074002 (2008).
19. C.D.White and R.S.Thorne, *Eur.Phys.J.C* **45**, 179 (2006).
20. A. Vogt, S. Moch and J.A.M. Vermaseren, *Nucl.Phys.B* **691**, 129 (2004).
21. W.L. van Neerven and A.Vogt, *Phys.Lett.B* **490**, 111 (2000).
22. M.A.G.Aivazis et al., *Phys.Rev.D* **50**, 3102 (1994).
23. A.V.Kotikov, B.G.Shaikhatdenov and Pengming Zhang, *Phys.Rev.D*96, 114002(2017); G.Beuf, C.Royon and D.Salek, arXiv [hep-ph]:0810.5082.
24. T.-J. Hou, et al., *Phys. Rev. D* **103**, 014013 (2021).
25. H. Abdolmaleki et al., *Eur. Phys. J. C* **78**, 621 (2018).
26. A.V. Kotikov, *JETP* **80**, 979 (1995); A.V. Kotikov, G. Parente, *Mod.Phys.Lett.A* **12**, 963 (1997).
27. E.A.Kuraev, L.N.Lipatov and V.S.Fadin, *ZHETF* **53**, 2018 (1976); **54**, 128 (1977); Ya.Ya.Balitzki and L.N.Lipatov, *Yad.Fiz.* **28**, 822 (1978); L.N.Lipatov, *ZHETF* **63**,904 (1986).
28. D.Britzger et al., *Phys. Rev. D* **100**, 114007 (2019).
29. C.Pisano, *Nuclear Physics B-Proceedings Supplements*, **186**, 47 (2009).

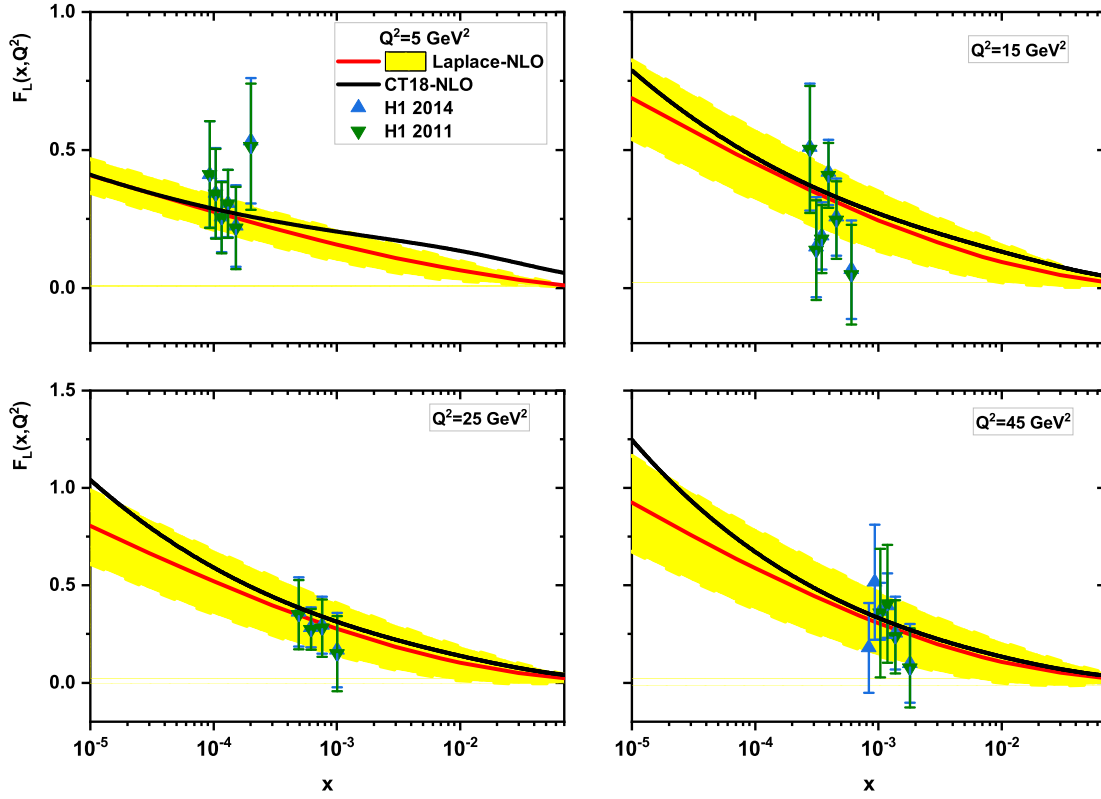


FIG. 1: The longitudinal structure function results at NLO approximation with respect to the Laplace transform method compared with the H1 experimental data (up and down triangles) [2] as accompanied with total errors and with the CT18 NLO [24] parametrization model. The error bands are due to the charm-quark mass uncertainty and the statistical errors in the parametrization of $F_2(x, Q^2)$ and its derivative.

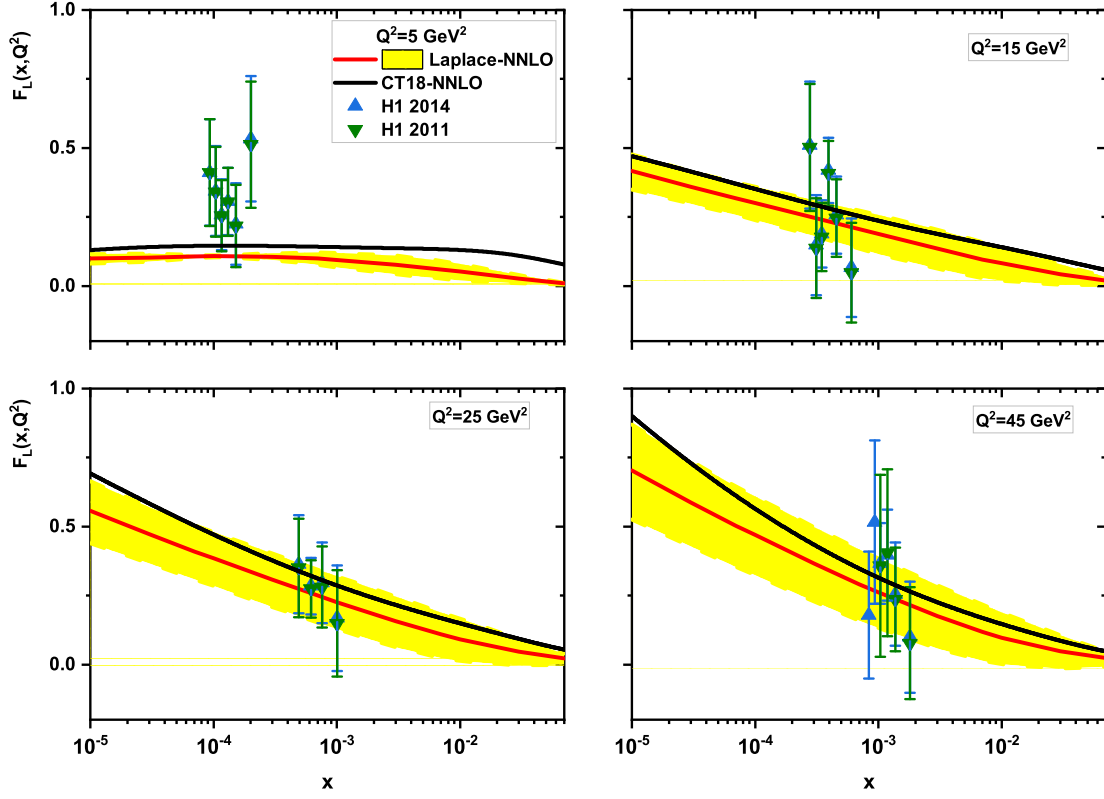


FIG. 2: The longitudinal structure functions at NNLO approximation with respect to the Laplace transform method extracted in comparison with the H1 experimental data (up and down triangles) [2] as accompanied with total errors. The error bands are due to the charm-quark mass uncertainty and the statistical errors in the parametrization of $F_2(x, Q^2)$ and its derivative. The results compared with the CT18 NNLO [24] parametrization model.

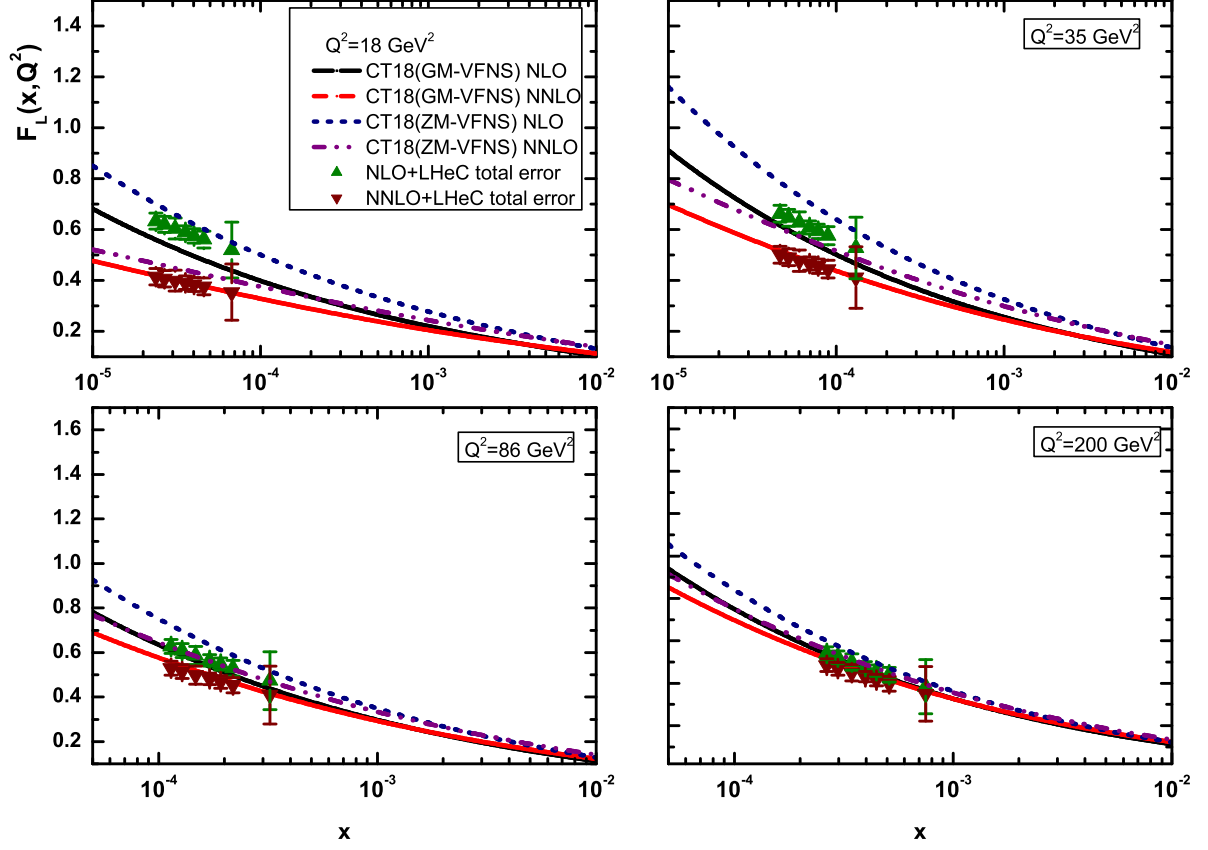


FIG. 3: The longitudinal structure function $F_L(x, Q^2)$ with respect to the LHeC simulated errors [9] in comparison with the results of CT18 NLO and NNLO models [24] in the GM-VFNS and ZM-VFNS at Q^2 values 18, 32, 86 and 200 GeV^2 .

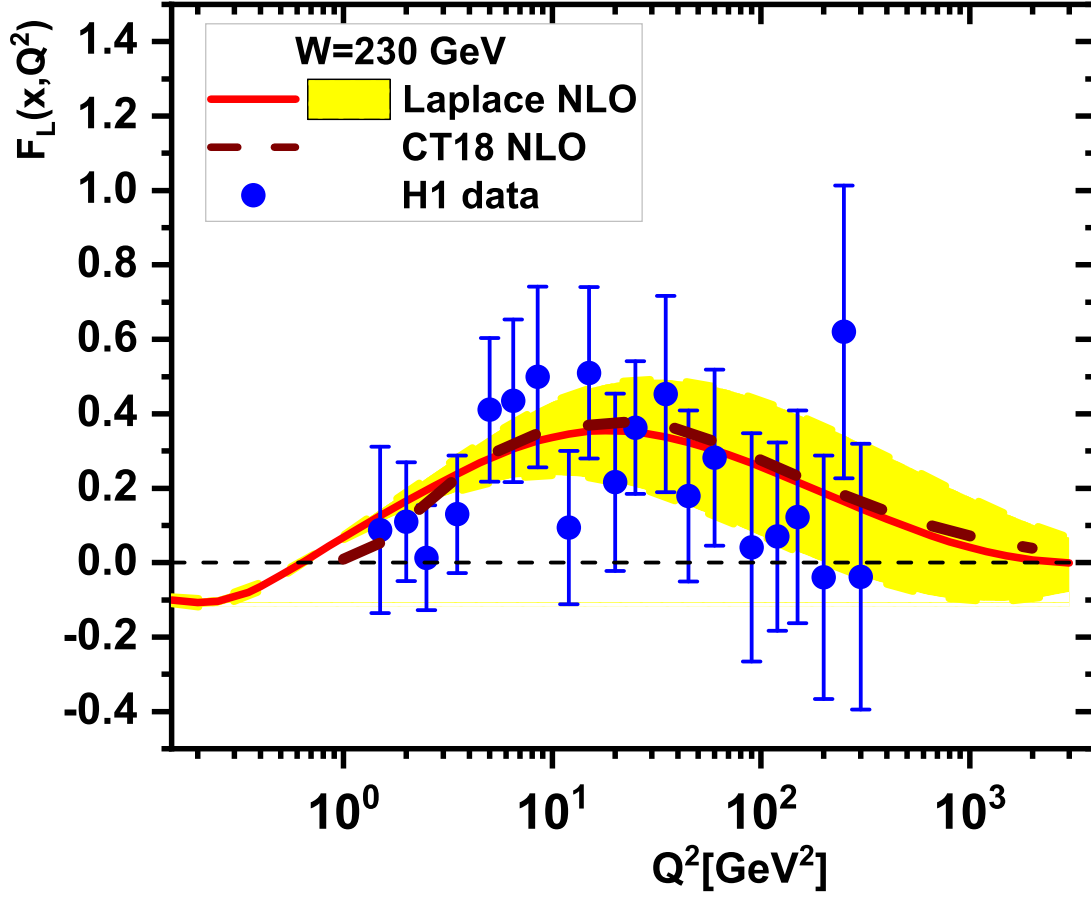


FIG. 4: The extracted longitudinal structure function $F_L(x, Q^2)$ from the parametrization of $F_2(x, Q^2)$ at fixed value of the invariant mass $W = 230$ GeV (solid curve) compared with the CT18 model [24] (dashed curve) in the NLO approximation. The error bands are due to the charm-quark mass uncertainty and the statistical errors in the parametrization of $F_2(x, Q^2)$ and its derivative. Experimental data are from the H1-Collaboration, Refs.[1,2] as accompanied with total errors.

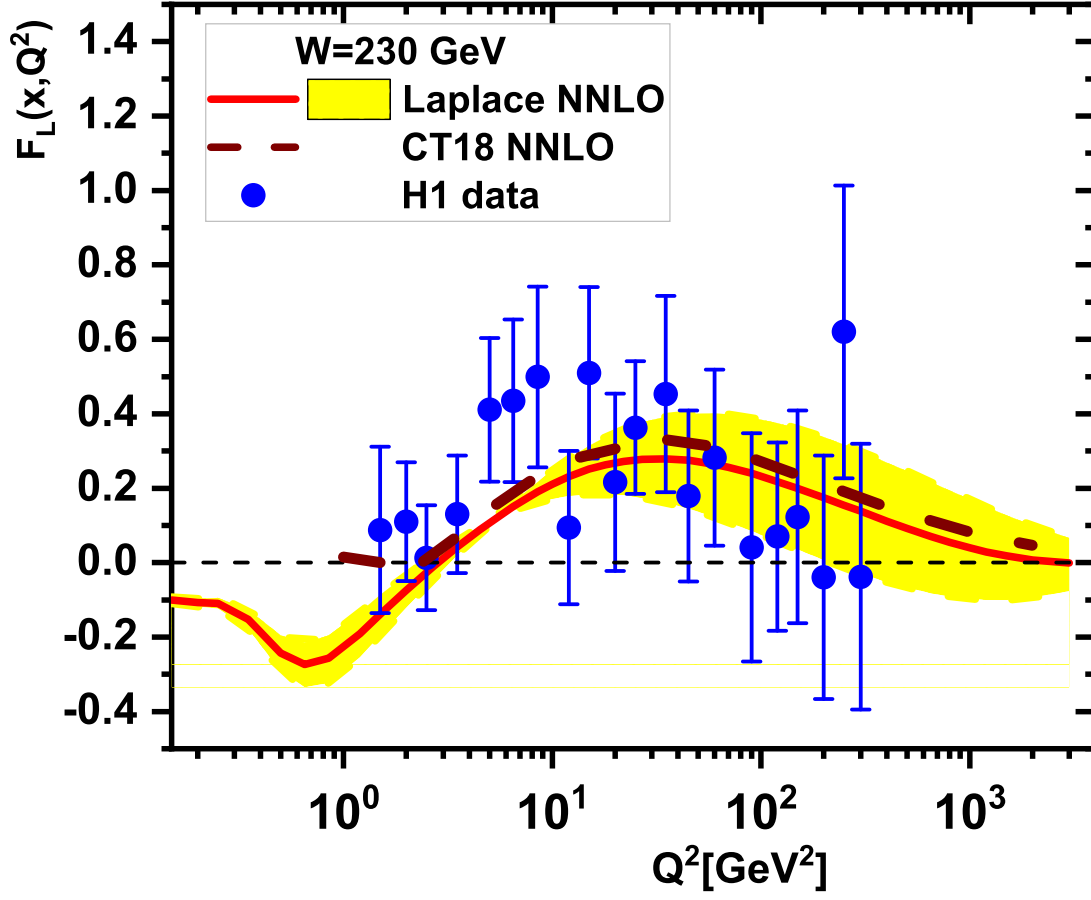


FIG. 5: The same as Fig.4 for the longitudinal structure function in the NNLO approximation at $W = 230$ GeV.

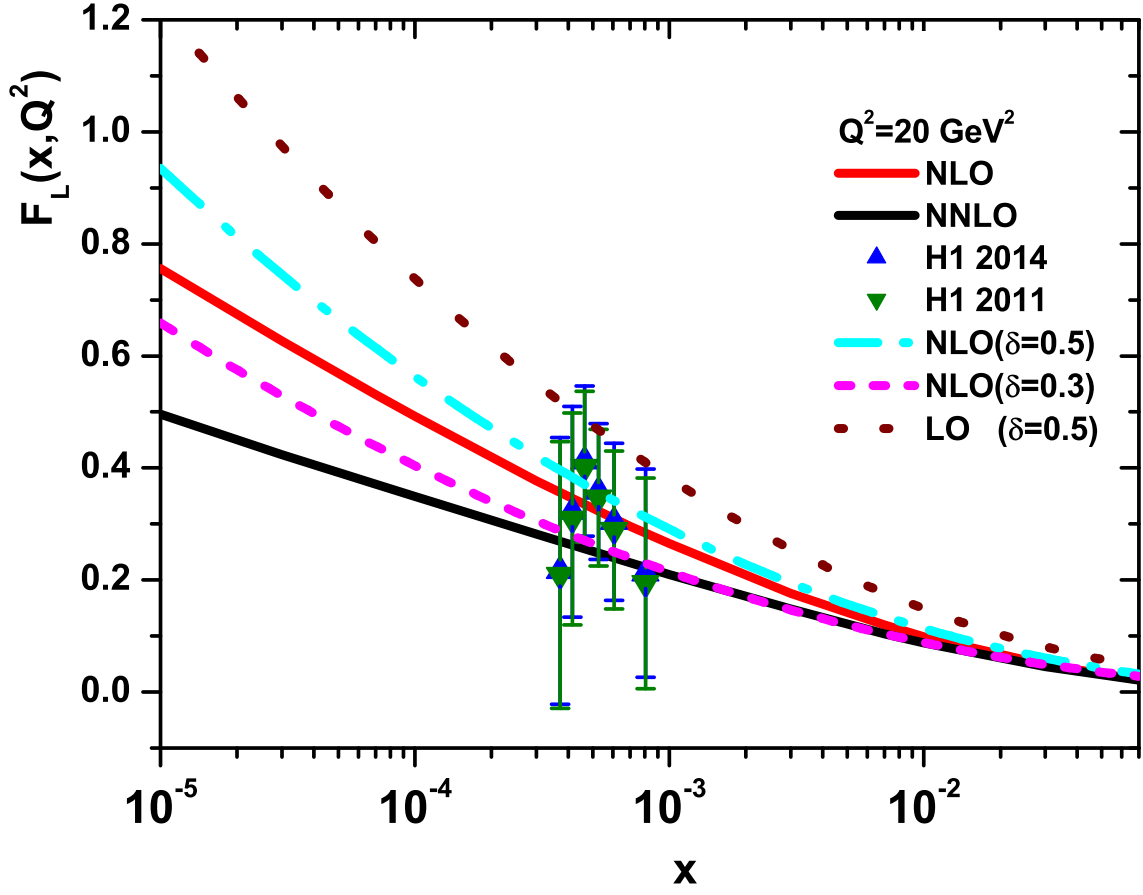


FIG. 6: The longitudinal structure functions at NLO and NNLO approximations (solid curves), by the Laplace transform method, and by the Regge-like behavior [26] at LO and NLO approximations (Dashed and dot curves) for $\delta = 0.5$ and 0.3 at $Q^2 = 20 \text{ GeV}^2$ compared with the H1 Collaboration data are taken from Refs.[1,2] as accompanied with total errors.

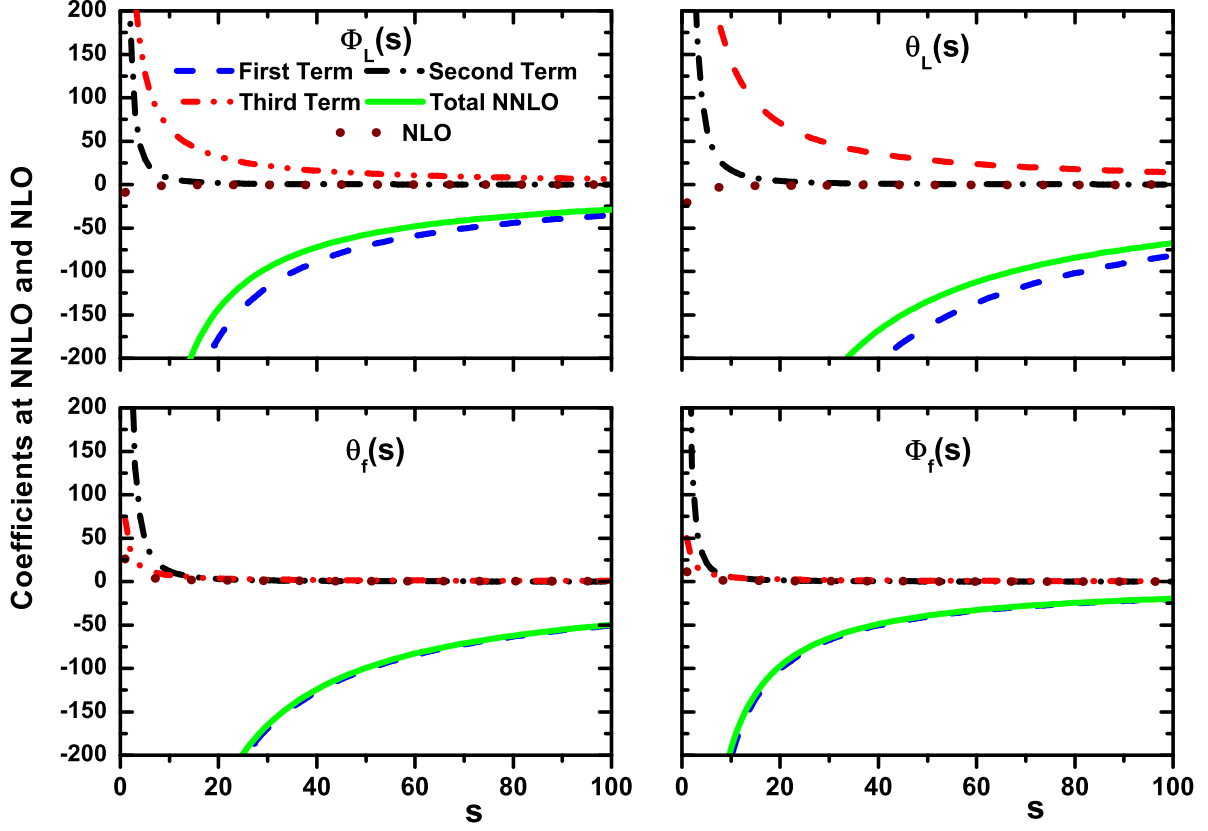


FIG. 7: The coefficient functions (i.e., Eqs.(14) and (15)) plotted at small x at NNLO and NLO approximations in s -space. The first, second and third terms at NNLO approximation are shown, also the total approximation coefficients at NLO (dot-curve) compared with NNLO (solid curve) in s -space.